A High-Performance Lithium-Ion Battery Anode by Direct Growth of Hierarchical ZnCo2O4 Nanostructures on Current Collectors.

6 AUTHORS, INCLUDING:

Baihua Qu
Xiamen University
30 PUBLICATIONS **790** CITATIONS

SEE PROFILE

Yanguo Wang
Hunan University
71 PUBLICATIONS **2,506** CITATIONS

SEE PROFILE

Libao Chen
Central South University
65 PUBLICATIONS **1,995** CITATIONS

SEE PROFILE

Taihong Wang
Hunan University
281 PUBLICATIONS **12,406** CITATIONS

SEE PROFILE

High-Performance Lithium-Ion Battery Anode by Direct Growth of Hierarchical ZnCo$_2$O$_4$ Nanostructures on Current Collectors

Baihua Qu,[†,§] Lingling Hu,[†,§] Qiuhong Li,[†] Yanguo Wang,[†,‡] Libao Chen,*[,†] and Taihong Wang*[,†]

[†]Key Laboratory for Micro-Nano Optoelectronic Devices of the Ministry of Education and State Key Laboratory of Chemo/Biosensing and Chemometrics, Hunan University, Changsha 410082, P. R. China

[‡]Institute of Physics, Chinese Academy of Sciences, P.O. Box 603, Beijing 100190, P. R. China

ABSTRACT: Hierarchical nanostructures that can be directly grown on a conducting substrate are a new trend in the design of active materials for high-performance lithium-ion batteries (LIBs). This article reports our design and fabrication of a 3D hierarchical ZnCo$_2$O$_4$ nanostructure (3D-ZCO-NS) directly grown on Ni foams. The goose-feather-like ZnCo$_2$O$_4$ bundled into a loose array structure with a large electrolyte contact area and good electrical and mechanical connection to the current collector. Electrochemical measurements confirmed the good performance of the electrode for reversible Li$^+$ storage (specific capacity of 932 mAh g^{-1} in the 50th cycle at 1 A g^{-1}) relative to a pasted electrode of 3D-ZCO-NSs (599 mAh g^{-1} in the 50th cycle at 0.1 A g^{-1}).

KEYWORDS: hierarchical nanostructures, direct growth, ZnCo$_2$O$_4$, lithium-ion battery
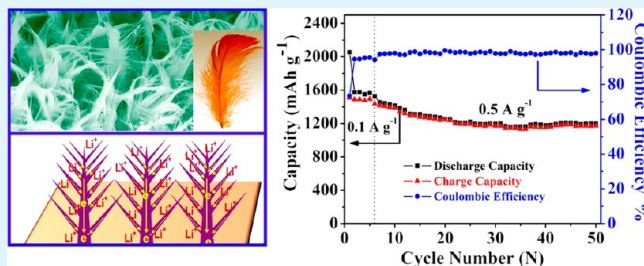
INTRODUCTION

Hierarchically structured materials with at least one dimension on the nanometer length scale (hierarchical nanostructures) can combine desirable bulk-material properties (e.g., structural stability and high tap density) with size-tunable functional properties for the construction of electrochemical energy-storage devices (LIBs and supercapacitors). The design of 3D hierarchical structures can leverage their unique size and shape for the facile transport of electrons and Li$^+$ in the solid state and their extensive surface area to increase the active material–electrolyte contact.[1−10] For example, 3D hierarchical Co$_3$O$_4$ nanostructures have been used for supercapacitors and have shown increased electrode stability as well as higher rates of ionic diffusion and electron transport in the fabricated devices.[5] Our recent work also demonstrated that the good Li$^+$-storage properties of branched Co$_3$O$_4$ nanostructures could be attributed to the formation of an interdigitated network in the electrode, where the backbone of the hierarchical structure was interlinked to form a continuous conducting network.[6]

However, many applications of these 3D hierarchical nanostructured materials involve mixing them with a conductive additive and polymer binder to form pasted electrodes on current collectors. The actual capacity of the electrode is lower than the specific capacity of the active material because of the presence of the inactive components (conductive additive and polymer binder). The latter also reduce electrolyte accessibility to the active material, resulting in less efficient Faradaic reactions for energy storage.[11] An alternative to the use of pasted electrodes in LIBs is the direct growth of ordered nanostructures on a conducting substrate. Aside from a simpler electrode fabrication process and better

electrical integration with the current collector, the direct-growth method also offers other benefits, such as fast electron transport and collection and ion diffusion as well as better accommodation of stress and strain in the materials because of the lithium insertion and de-insertion reactions. Consequently, there is increasing interest in directly using growth-ordered nanostructures to improve electrochemical performance.[12−19] For example, Wu and co-workers[12] reported the growth of self-supporting mesoporous Co$_3$O$_4$ nanowire arrays on different conducting substrates. Good electrochemical performance was shown and attributed to the good contact of each nanowire with the conducting substrate and with the electrolyte solution. Very high specific capacity and rate capability were also reported for the anode of Co$_3$O$_4$ nanobelt arrays grown directly on Ti foil.[13] The porous Co$_3$O$_4$ nanoneedle arrays of Xue et al. grown directly on copper foil also exhibited ultrafast charging and discharging in LIBs.[14] Again, the reasons for this were the good contact with the current collector and short electron-transport paths.

Recently, there has been interest in ternary ZnCo$_2$O$_4$ as a cheaper and environmentally more acceptable alternative to binary Co$_3$O$_4$ as a LIB anode material.[20−31] The theoretically higher lithiation capacity of ZnCo$_2$O$_4$ ($\sim$976 mAh g^{-1}) could be attributed to the combination of two conversion reactions (those of Zn and Co oxides). Furthermore, Zn could also undergo alloying and de-alloying reactions with Li.[20,24] The incorporation of a third element, Zn, could improve the cycling

performance owing to possible synergetic interactions between Co and Zn, and the presence of cobalt oxide in the ZnO matrix could be mutually beneficial.[20,22,32−35] In the past several years, $ZnCo_2O_4$ has been fabricated as nanoparticles,[20−22,24] porous nanowires,[23] porous nanotubes,[25] and nanorods[27] for use in pasted electrodes on current collectors. However, the rate performance and cycle stability of $ZnCo_2O_4$ pasted electrodes appear to have reached the limits of pasted-electrode technology. The direct growth of $ZnCo_2O_4$ on conducting substrates may be a solution for further improving the performance of $ZnCo_2O_4$. This article reports the design and fabrication of feather-like 3D hierarchical nanostructures of $ZnCo_2O_4$ directly on Ni foams (3D-ZCO-NSs/Ni) current collectors, which can be used as binder-free electrodes with high specific capacity and good cycle stability and rate performance. Specifically, the 3D-ZCO-NSs/Ni-foam electrodes fabricated as such could deliver discharge (lithiation) capacities of at least 1100 mAh g^{-1} for 50 cycles at 0.5A g^{-1} and 932 mAh g^{-1} for 50 cycles at 1 A g^{-1}.

■ EXPERIMENTAL SECTION

Synthesis of 3D-ZCO-NSs/Ni Foams. Zinc acetate dihydrate $(Zn(CH_3COO)_2 \cdot 2H_2O)$, cobalt acetate tetrahydrate (Co-$(CH_3COO)_2 \cdot 4H_2O)$, ammonium fluoride (NH_4F), urea (CO-$(NH_2)_2)$, hydrochloric acid (HCl), ethanol, and carboxymethyl cellulose (CMC) were obtained from Shanghai Chemical Reagent Co. All chemicals were of analytical grade and used without further purification. Deionized water with resistivity higher than 18.2 MΩ cm was used as a common solvent. 3D-ZCO-NSs supported on Ni foams (Changsha Lyrun Material Co., Ltd. China) were prepared by a template-free growth method. In a typical experiment, a Ni-foam substrate (length × with × thickness =10 × 5 × 0.1 cm^3) after degreasing in ethanol was etched in 3 M HCl for 20 min. After washing with deionized water and ethanol and drying, the Ni foam was placed against the wall of a Teflon-lined autoclave (130 mL). The back of the Ni foam was covered by polytetrafluoroethylene tape to inhibit the growth of nanostructures there. Independently, a mixture of 2 mmol $Zn(CH_3COO)_2 \cdot 2H_2O$, 4 mmol $Co(CH_3COO)_2 \cdot 4H_2O$, 4 mmol NH_4F, and 10 mmol $CO(NH_2)_2$ in 80 mL of distilled water and 20 mL of ethanol was prepared and magnetically stirred for 1 h at room temperature before it was transferred to the Teflon-lined autoclave and hydrothermally processed in an oven for 16 h at 120°C before cooling to room temperature naturally. The recovered Ni-foam-supported product was ultrasonicated in deionized water and ethanol several times to remove residual nanoparticle debris followed by drying at 60 °C for 8 h. The precipitate in the solution was also collected and washed with distilled water and ethanol before drying at 60 °C for 8 h. The coated Ni foam was then annealed at 400 °C in Ar for 2 h. The annealed, blackened Ni foam was designated as 3D-ZCO-NSs/Ni. A black 3D-ZCO-NSs powder was also obtained by annealing the powder in Ar at 400 °C for 2 h.

Structure and Morphology Characterizations. The materials in this study were characterized by X-ray powder diffraction (XRD) on a SIEMENS D5000 X-ray diffractometer with Cu Kα radiation (λ=1.5408 Å). Product morphology and structure were analyzed by scanning electron microcopy (SEM, Hitachi S4800) and transmission electron microscopy (TEM, JEOL-2010). High-resolution transmission electron microscopy (HRTEM), elemental mapping by energy-dispersive X-ray spectroscopy (EDX), and selected-area electron diffraction (SAED) were performed on a JEM-2100F (JEOL) system operating at 200 kV.

Electrochemical Measurements. The electrochemical properties of the products were measured in CR 2025-type coin cells. The Ni-foam-supported 3D-ZCO-NSs was vacuum dried at 80 °C for 12 h to remove residual water before it was used as the working electrode. For the coin-cell assembly, the $ZnCo_2O_4$-coated Ni foams were punched into 16 mm diameter disc electrodes and used without conductive

additive and polymer binder. The loading of the active material on the electrode was about 4 mg (2 mg cm^{-2}). One molar $LiPF_6$ in a mixture of ethylene carbonate (EC), dimethyl carbonate (DMC), and ethyl methyl carbonate (EMC) (EC/DMC/EMC = 1:1:1 v/v/v) was used as the electrolyte. The assembly of test cells was performed in an Ar-filled glove box where water and oxygen content was less than 1 ppm each. A pure Li foil was used as the counter electrode, and a polypropylene (PP) film (Celgard 2400) was used as the separator.

For the comparative study of electrochemical performance, the 3D-ZCO-NSs powder was also formed into working electrodes. The pasted electrode was prepared in the usual way[36] by mixing 80 wt % of the active material with 10 wt % each of the conductivity agent (carbon black, Super-P-Li) and binder (carboxymethyl cellulose, CMC) in a mixture of distilled water and absolute alcohol into a uniform slurry. The homogenized slurry was then applied uniformly onto a copper foil and dried at 80 °C in a vacuum oven for 12 h.

Electrochemical measurements were carried out on a multichannel Arbin Instruments BT 2000 (USA) unit in the 0.01−3.00 V range. Electrochemical impedance spectroscopy (EIS) was performed on a CHI660D (Shanghai Chenhua Device Company, China) electrochemistry workstation, and cyclic voltammetry (CV) was measured on an AutoLab FRA2 type III electrochemical system at the scan rate of 0.1 mV s^{-1} in the range of 0−3 V.

■ RESULTS AND DISCUSSION

Figure 1a shows a Ni foam and Ni foam deposited with 3D-ZCO-NSs before and after heat treatment. Figure 2 shows the
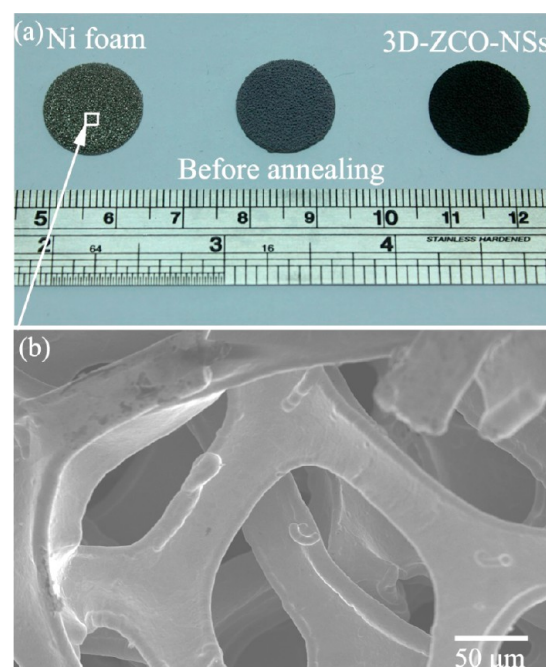

Figure 1. (a) Optical image of the Ni foam before and after the annealing of 3D-ZCO-NSs. (b) SEM image of the Ni foam.

results of electron microscopy characterization of the morphology and structure of the 3D-ZCO-NSs. The low-magnification scanning electron microscope (SEM) image of 3D-ZCO-NSs/Ni in Figure 2a shows that the Ni-foam skeleton was coated with goose-feather-like products. However, from SEM image of Figure 1b, it can be seen that there is a smooth surface on the Ni foam before coating. The zoomed-in view of the SEM image (Figure 2b) discloses the hierarchical structure of the goose feathers, where multiple rows of secondary nanowires were grown on approximately parallel micrometer shafts. These feather-like hierarchical nanostructures could
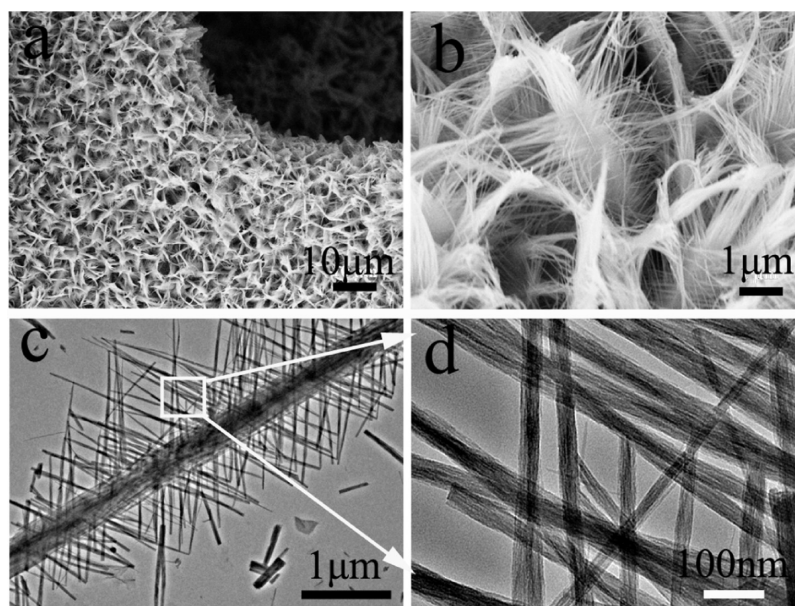
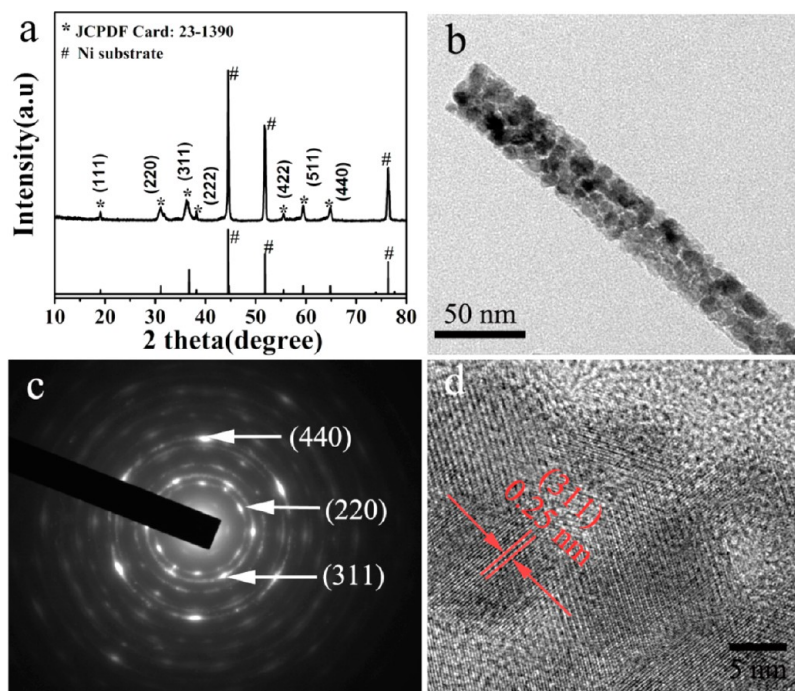**Figure 2.** (a) Low-magnification SEM image, (b) high-magnification SEM image, and (c, d) TEM image of 3D-ZCO-NSs.

Figure 3. (a) XRD pattern of annealed 3D-ZCO-NSs. (b) Typical TEM image of a $ZnCo_2O_4$ branch. (c) SAED pattern of a $ZnCo_2O_4$ branch. (d) HRTEM image of a $ZnCo_2O_4$ branch.

grow to a very high density perpendicular to the substrate. The finer details of the hierarchical structure were revealed by transmission electron microscopy (TEM) using 3D-ZCO-NSs, which were removed from the Ni-foam substrate. Figure 2c shows the nanowire-like branches that were assembled around a typical shaft. The average diameter of the nanowire-like branches was about 50 nm (Figure 2d).

The crystal structure and phase purity of the 3D-ZCO-NSs/Ni were determined from the XRD pattern in Figure 3a. There are three diffraction peaks from the Ni foam (marked with a # symbol) and seven diffraction peaks (marked with a * symbol) that associate well with the (111), (220), (311), (222), (422),

(511), and (440) planes of the $ZnCo_2O_4$ cubic spinel structure ($a = 8.0946$ Å, space group: $Fd-3m$, JCPDS card no. 23-1390).[20,22] The absence of other diffraction peaks indicates the formation of phase-pure $ZnCo_2O_4$ after thermal annealing. Figure 3b is a representative TEM image of a $ZnCo_2O_4$ nanowire-like branch after heat treatment. It shows the branch as an ensemble of 10−14 nm nanocrystals that are packed into a compact linear structure. Pores could, however, be seen between the constituent $ZnCo_2O_4$ nanoparticles and hence the actual surface-to-volume ratio was higher than what is calculated from the overall aspect ratio. The porosity created as such is beneficial to electrolyte penetration. d values of 0.28,

733

dx.doi.org/10.1021/am405238a | ACS Appl. Mater. Interfaces 2014, 6, 731−736

0.25, and 0.14 nm, corresponding well with the (220), (311), and (440) diffractions of $ZnCo_2O_4$, could be calculated from the selected-area electron diffraction (SAED) pattern in Figure 3c. The HRTEM image of an isolated $ZnCo_2O_4$ nanowire-like branch is given in Figure 3d. The lattice fringes with a separation of 0.25 nm from the constituent nanoparticles could be indexed to the $ZnCo_2O_4$ (311) crystal plane, which is in good agreement with the most intense diffraction peak in the XRD pattern. Scanning TEM energy-dispersive X-ray spectroscopy (EDS) was used to determine the elemental composition and the spatial uniformity of the elemental distribution on the nanoscale. The results in Figure 4 show that Zn, Co, and O atoms were evenly distributed over the length and width of the nanowire-like branch.
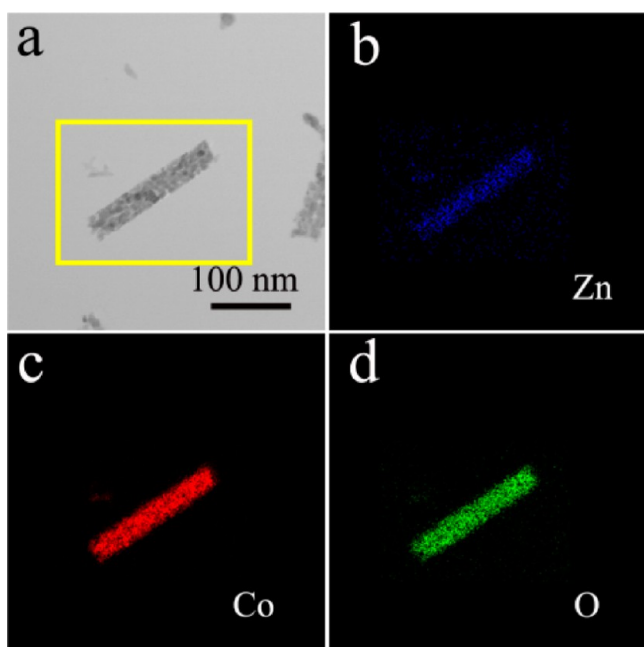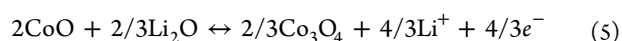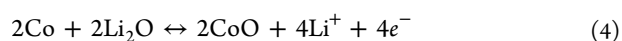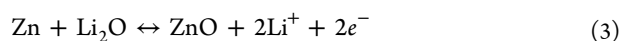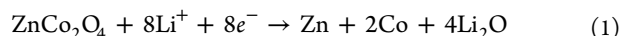

Figure 4. (a) STEM image of the $ZnCo_2O_4$ nanowire along with the corresponding elemental maps of (b) Zn, (c) Co, and (d) O.

The electrochemical performance of the 3D-ZCO-NSs/Ni foams as a conductivity-agent-free and binder-free anode for LIBs was evaluated by cyclic voltammetry (CV) and galvanostatic discharging and charging. CV measurements were carried out at a scan rate of 0.1 mV s^{-1} over the 0–3.0 V voltage range. As shown in Figure 5a, there was a shoulder peak at ~1.0 V in the first cathodic process. The underlying reduction reaction was most likely the decomposition of $ZnCo_2O_4$ to Zn^0 and Co^0 according to eq 1. The intense peak at ~0.6 V could be assigned to the decomposition of $ZnCo_2O_4$ to Zn^0 and Co^0 according to eq 1 and the formation of a solid electrolyte interphase (SEI).[21,23–25] Two broad oxidation peaks were found at ~1.5 and ~2.2 V in the first anodic scan, which could be attributed to the oxidation of Zn^0 to Zn^{2+} and Co^0 to Co^{3+} (eqs 3–5), respectively. The overlapping CV profiles after the first cycle indicate good electrochemical reversibility of the 3D-ZCO-NSs/Ni foam for Li$^+$ insertion and extraction from the second cycle onwards. The discharge and charge curves at 0.1 A g^{-1} (for the first five cycles) are shown in Figure 5b. The abrupt voltage drop to ~1.0 V in the first discharge curve was due to the conversion reaction in eq 1 and is consistent with the CV measurement.[24] The broad potential plateau at 0.75 V

has been thoroughly discussed in previous literature.[20–28] The long potential plateau was replaced by a sloping discharge curve from the 2nd cycle onwards and good superimposition (e.g., the 2nd and the 5th cycles), indicating that a stable SEI could be formed in the first cycle.[22] The good reiteration of the charge and discharge curves after the first cycle also indicates good electrochemical reversibility in the reduction–oxidation and alloying–de-alloying (LiZn) reactions and is consistent with the CV results. The initial discharge and charge capacities were 2053 and 1508 mAh g^{-1}, respectively. The superimposition of the voltage profiles for the 2nd to the 5th cycle suggests good electrochemical cyclability of the 3D-ZCO-NSs/Ni foam. The following reactions are usually used to describe the electrochemistry of a $ZnCo_2O_4$ electrode. Reactions 3–5 in particular are responsible for the reversibility in discharge and charge.[20–29]

$$ZnCo_2O_4 + 8Li^+ + 8e^- \rightarrow Zn + 2Co + 4Li_2O \tag{1}$$

$$Zn + Li^+ + e^- \leftrightarrow LiZn \tag{2}$$

$$Zn + Li_2O \leftrightarrow ZnO + 2Li^+ + 2e^- \tag{3}$$

$$2Co + 2Li_2O \leftrightarrow 2CoO + 4Li^+ + 4e^- \tag{4}$$

$$2CoO + 2/3Li_2O \leftrightarrow 2/3Co_3O_4 + 4/3Li^+ + 4/3e^- \tag{5}$$

The cycling performance of the electrode over 50 cycles of charge and discharge is shown in Figure 5c. The current density increased to 0.5 A g^{-1} in the 6th cycle, and discharge and charge capacities of 1523 and 1435 mAh g^{-1}, respectively, were obtained. The fading of the capacity thereafter was much slower, and a specific capacity above 1100 mAh g^{-1} was sustainable at this current density for 50 cycles. The low first-cycle Coulombic efficiency of 73.5% was superseded by a much higher value of 97% in the subsequent cycles.

For comparison, the performance of a 3D-ZCO-NSs pasted electrode was also measured. The initial discharge capacity and Coulombic efficiency recorded at 0.1 A g^{-1} were only marginally lower, at 1435 mAh g^{-1} and 71%, respectively (Figure 5d). The difference came only after the first cycle; the discharge capacity faded very quickly in the first seven cycles (from 1435 to 878 mAh g^{-1}) before the fade rate stabilized to a smaller and more constant value. Consequently, the measured capacities were noticeably lower than those of 3D-ZCO-NSs directly grown on the Ni foam. The specific capacity at the end of the 50th cycle was only 599 mAh g^{-1}, about 55% of the capacity of 3D-ZCO-NSs/Ni measured at a much higher current density of 0.5 A g^{-1} in the same number of cycles. Figure 6 shows the cycle stability of 3D-ZCO-NSs/Ni at higher current densities. Using the 50th cycle discharge capacity at 0.5 A g^{-1} (1122 mAh g^{-1}) as the reference point, the corresponding values at the higher current densities of 1 and 2 A g^{-1} were ~932 and 542 mAh g^{-1}, respectively. These measurements confirm the merits of the 3D-ZCO-NSs/Ni electrode over a 3D-ZCO-NSs pasted electrode. Furthermore, the Li$^+$-storage capacity and rate performance of 3D-ZCO-NSs/Ni are superior to most $ZnCo_2O_4$ pasted electrodes.[20–28]

The high capacity and good rate performance of 3D-ZCO-NSs/Ni may be attributed to its two unique features: a feather-like 3D hierarchical structure and direct growth on the current collector. The branches in the 3D hierarchical structure significantly increased the accessibility of the charge–discharge sites to Li$^+$. This was complemented by an efficient electron
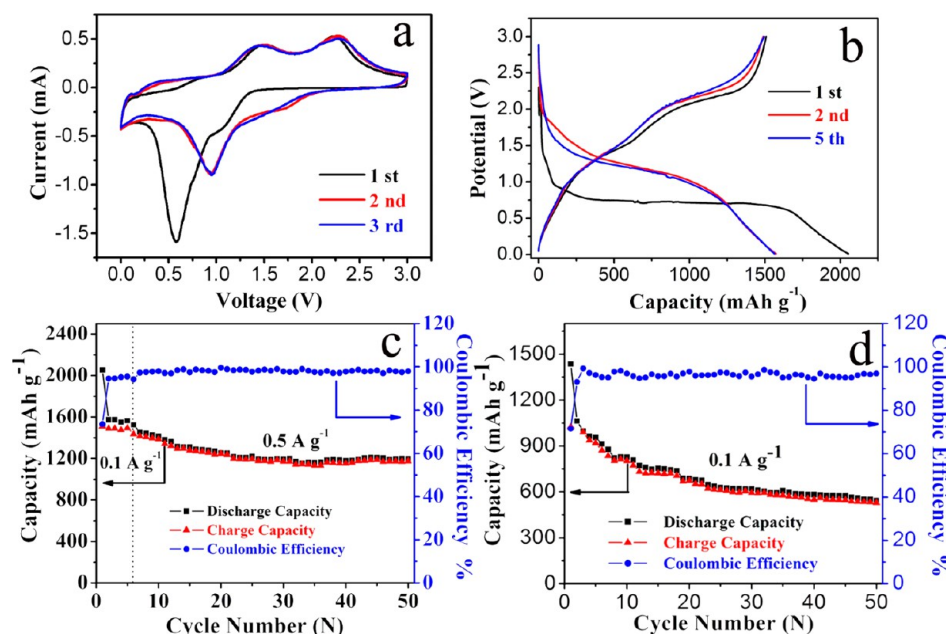
Figure 5. (a) First three CVs of the 3D-ZCO-NSs/Ni foam at a scan rate of 0.1 mV s^{-1}. (b) First, 2nd, and 5th cycle discharge−charge curves of the 3D-ZCO-NSs/Ni foam at a current density of 0.1 A g^{-1} in the 0.01−3 V window. (c) Cycling performance of the 3D-ZCO-NSs/Ni foam at 0.5 A g^{-1} (for the first 5 cycles at 0.1 A g^{-1}). (d) Cycling performance of the 3D-ZCO-NSs pasted electrode at 0.1 A g^{-1}.
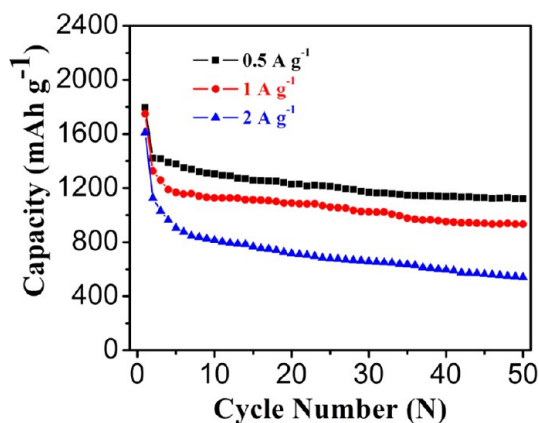

Figure 6. Cycling performance of 3D-ZCO-NSs/Ni foam at different current densities.

conduction and collection to the current collector provided by the stalks of the feather-like structure (Figure 7a). The feather-like structure also increased the void space to accommodate the volume changes in the Li$^+$ insertion and extraction reactions. Electron collection and conduction and strain relief are effective only if the hierarchical structure is orderly so that random overlap is reduced and good contact with the current collector is made. Both of these conditions were satisfied by the direct-

growth method. A pasted electrode (Figure 7b) cannot ensure the direct contact of the active material with the current collector or preserve the quality of the adhesion if the binder and conductive additive are subjected to cyclical changes in the volume, stress, and strain of the active material. The randomness in the arrangement of the hierarchical structures also increased the diffusion lengths for electrons and Li$^+$. Furthermore, the presence of binder could also impede electron conduction between the active material and the current collector because most binders with good adhesion properties are electron insulators.

The directly grown and pasted 3D-ZCO-NSs electrodes were also characterized by electrochemical impedance spectroscopy (EIS) to evaluate their susceptibility to structural degradation with repeated discharging and charging. The results, presented as Nyquist plots (Figure 8), show the usual feature of a semicircle in the high-frequency region and an inclined straight line in the low-frequency region. It is worth noting that the charge-transfer resistance (as measured by the size of the high-frequency semicircle) of the direct-growth structure (125 Ω) was smaller than that of the pasted electrode (160 Ω) in the initial, as-assembled state of the test cell. Furthermore, the increase in charge-transfer resistance after prolonged cycling, which measures the structural integrity of the electrode, was smaller for the direct-growth electrode (260% after 50 cycles)
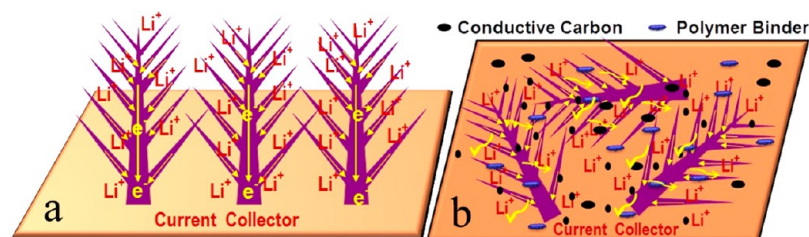

Figure 7. Schematic comparisons of 3D-ZCO-NSs (a) directly grown and (b) pasted on a current collector.
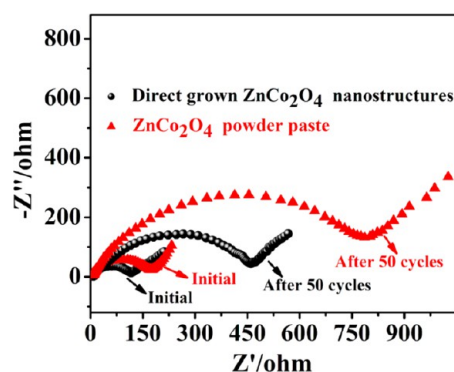
Figure 8. Nyquist plots of 3D-ZCO-NSs directly grown vs pasted on the current collector for the 1st and 50th cycles.

than the pasted electrode (400% after 50 cycles). Hence, the direct-growth electrode was able to preserve the integrity better and consequently the benefits of the 3D-ZCO-NSs structure. Thus, it is a better deployment technique than the pasted electrode.

■ CONCLUSIONS

A 3D $ZnCo_2O_4$ hierarchical nanostructure was grown directly on a Ni-foam substrate to form a conductivity-agent-free and binder-free electrode suitable for use as the anode of LIBs. Very good cyclability and rate performance were shown relative to the use of the same hierarchically structured material in pasted electrodes. The good electrochemical performance could be attributed to the hierarchical structure that increased the accessible area for Li^+ exchange with the storage host, the free volume for relieving the stress in the active material during cycling, and the effective collective and conduction of electrons to the current collector as well as the ordered structure, which maximized these effects.

■ AUTHOR INFORMATION

Corresponding Authors
*E-mail: lbchen@hnu.edu.cn (L.C.).
*E-mail: thwang@hnu.edu.cn (T.W.).

Author Contributions
§These authors contributed equally.

Notes
The authors declare no competing financial interest.

■ ACKNOWLEDGMENTS

■ REFERENCES

(1) Yu, Y.; Gu, L.; Zhu, C. B.; Tsukimoto, S.; Aken, P. A. V.; Maier, J. *Adv. Mater.* **2010**, *22*, 2247−2250.

(2) Park, M. H.; Kim, K.; Kim, J.; Cho, J. *Adv. Mater.* **2010**, *22*, 415−418.

(3) Zhou, W. W.; Cheng, C. W.; Liu, J. P.; Tay, Y. Y.; Jiang, J.; Jia, X. T.; Zhang, J. X.; Gong, H.; Hng, H. H.; Yu, T.; Fan, H. J. *Adv. Funct. Mater.* **2011**, *21*, 2439−2445.

(4) Shen, L. F.; Uchaker, E.; Yuan, C. Z.; Nie, P.; Zhang, M.; Zhang, X. G.; Cao, G. Z. *ACS Appl. Mater. Interfaces* **2012**, *4*, 2985−2992.

(5) Xiao, Y. H.; Liu, S. J.; Li, F.; Zhang, A. Q.; Zhao, J. H.; Fang, S. M.; Jia, D. Z. *Adv. Funct. Mater.* **2012**, *22*, 4052−4059.

(6) Li, C. C.; Yin, X. M.; Chen, L. B.; Li, Q. H.; Wang, T. H. *Appl. Phys. Lett.* **2012**, *10*, 209901−209903.

(7) Kim, H. J.; Kim, M. G.; Cho, J. *Adv. Energy Mater* **2012**, *2*, 1425−1432.

(8) Li, X. F.; Dhanabalan, A.; Gu, L.; Wang, C. L. *Adv. Energy Mater.* **2012**, *2*, 238−244.

(9) Pan, A. Q.; Wu, H. B.; Yu, L.; Zhu, T.; Lou, X. W. *ACS Appl. Mater. Interfaces* **2012**, *4*, 3874−3879.

(10) Li, L. L.; Cheah, Y. L.; Ko, Y. W.; Teh, P. F.; Wee, G.; Wong, C. L.; Peng, S. J; Sriniwasan, M. *J. Mater. Chem. A* **2013**, *1*, 10935−10941.

(11) Jiang, J.; Li, Y. Y.; Liu, J. P.; Huang, X. T. *Nanoscale* **2011**, *3*, 45−58.

(12) Li, Y. G.; Tan, B.; Wu, Y. Y. *Nano Lett.* **2008**, *8*, 265−270.

(13) Wang, Y.; Xia, H.; Lu, L.; Lin, J. Y. *ACS Nano* **2010**, *4*, 1425−1432.

(14) Xue, X. Y.; Yuan, S.; Xing, L. L.; Chen, Z. H.; He, B.; Chen, Y. J. *Chem. Commun.* **2011**, *47*, 4718−4720.

(15) Liu, J. P.; Li, Y. Y.; Fan, H. J.; Zhu, Z. H.; Jiang, J.; Ding, R. M.; Hu, Y. Y.; Huang, X. T. *Chem. Mater.* **2010**, *22*, 212−217.

(16) Li, C. C.; Li, Q. H.; Chen, L. B.; Wang, T. H. *J. Mater. Chem.* **2011**, *21*, 11867−11872.

(17) Xia, X. H.; Tu, J. P.; Zhang, Y. Q.; Chen, J.; Wang, X. L.; Gu, C. D.; Guan, C.; Luo, J. S.; Fan, H. J. *Chem. Mater.* **2012**, *24*, 3793−3799.

(18) Shen, L. F.; Uchaker, E.; Zhang, X. G.; Cao, G. Z. *Adv. Mater.* **2012**, *24*, 6502−6506.

(19) Wang, X. H.; Qiao, L.; Sun, X. L.; Li, X. W.; Hu, D. K.; Zhang, Q.; He, D. Y. *J. Mater. Chem. A* **2013**, *1*, 4173−4176.

(20) Sharma, Y.; Sharma, N.; Rao, G. V. S.; Chowdari, B. V. R. *Adv. Funct. Mater.* **2007**, *17*, 2855−2861.

(21) Qiu, Y. C.; Yang, S. H.; Deng, H.; Jin, L. M.; Li, W. S. *J. Mater. Chem.* **2010**, *20*, 4439−4444.

(22) Deng, D.; Lee, J. Y. *Nanotechnology* **2011**, *22*, 355401−355409.

(23) Du, N.; Xu, Y. F.; Zhang, H.; Yu, J. X.; Zhai, C. X.; Yang, D. *Inorg. Chem.* **2011**, *50*, 3320−3324.

(24) Reddy, M. V.; Kenrick, K. Y. H.; Wei, T. Y.; Chong, G. Y.; Leong, G. H.; Chowdari, B. V. R. *J. Electrochem. Soc.* **2011**, *158*, A1423−A1430.

(25) Luo, W.; Hu, X. L.; Sun, Y. M.; Huang, Y. H. *J. Mater. Chem.* **2012**, *22*, 8916−8921.

(26) Hu, L. L.; Qu, B. H.; Li, C. C.; Chen, Y. J.; Mei, L.; Lei, D. N.; Chen, L. B.; Li, Q. H.; Wang, T. H. *J. Mater. Chem. A* **2013**, *1*, 5596−5602.

(27) Liu, H. W.; Wang, J. *Electrochim. Acta* **2013**, *92*, 371−375.

(28) Xie, Q. S.; Li, F.; Guo, H. Z.; Wang, L. S.; Chen, Y. Z.; Yue, G. H.; Peng, D. L. *ACS Appl. Mater. Interfaces* **2013**, *5*, 5508−5517.

(29) Liu, B.; Zhang, J.; Wang, X. F.; Chen, G.; Chen, D.; Zhou, C. W.; Shen, G. Z. *Nano Lett.* **2012**, *12*, 3005−3011.

(30) Liu, B.; Wang, X. F.; Liu, B. Y.; Wang, Q. F.; Tang, D. S.; Song, W. F.; Hou, X. J.; Chen, D.; Shen, G. Z. *Nano Res.* **2013**, *6*, 525−534.

(31) Li, J. F.; Wang, J. Z.; Wexler, D.; Shi, D. Q.; Liang, J. W.; Liu, H. K.; Xiong, S. L.; Qian, Y. T. *J. Mater. Chem. A* **2013**, *1*, 15292−15299.

(32) Courtel, F. M.; Duncan, H.; Abu-lebdeh, Y.; Davidson, I. J. *J. Mater. Chem.* **2011**, *21*, 10206−10218.

(33) Li, J. F.; Xiong, S. L.; Liu, Y. R.; Ju, Z. C.; Qian, Y. T. *ACS Appl. Mater. Interfaces* **2013**, *5*, 981−988.

(34) Li, L. L.; Peng, S. J; Cheah, Y. L.; Ko, Y. W.; Teh, P. F.; Wee, G.; Wong, C. L.; Sriniwasan, M. *Chem.—Eur. J.* **2013**, *19*, 14823−14830.

(35) Li, J. F.; Xiong, S. L.; Li, X. W.; Qian, Y. T. *Nanoscale* **2013**, *5*, 2045−2054.

(36) Qu, B. H.; Li, H. X.; Zhang, M.; Mei, L.; Chen, L. B.; Wang, Y. G.; Li, Q. H.; Wang, T. H. *Nanoscale* **2011**, *3*, 4389−4393.